TGF-β signaling underlies hematopoietic dysfunction and bone marrow failure in Shwachman-Diamond syndrome

Cailin E. Joyce,[1,2] Assieh Saadatpour,[3,4] Melisa Ruiz-Gutierrez,[5] Ozge Vargel Bolukbasi,[5] Lan Jiang,[3,4] Dolly D. Thomas,[1,2] Sarah Young,[6] Inga Hofmann,[5] Colin A. Sieff,[5] Kasiani C. Myers,[7] Jennifer Whangbo,[5] Towia A. Libermann,[2,8] Chad Nusbaum,[6] Guo-Cheng Yuan,[3,4] Akiko Shimamura,[5] and Carl D. Novina[1,2,6]

[1]Department of Cancer Immunology and Virology, Dana-Farber Cancer Institute, Boston, Massachusetts, USA. [2]Department of Medicine, Harvard Medical School, Boston, Massachusetts, USA. [3]Department of Biostatistics and Computational Biology, Dana-Farber Cancer Institute, Boston, Massachusetts, USA. [4]Department of Biostatistics, Harvard T.H. Chan School of Public Health, Boston, Massachusetts, USA. [5]Division of Hematology/Oncology, Boston Children's Hospital and Dana-Farber Cancer Institute, Boston, Massachusetts, USA. [6]Broad Institute of Harvard and MIT, Cambridge, Massachusetts, USA. [7]Division of Bone Marrow Transplantation and Immune Deficiency, Cincinnati Children's Hospital Medical Center, Cincinnati, Ohio, USA. [8]Beth Israel Deaconess Medical Center Genomics, Proteomics, Bioinformatics and Systems Biology Center, Division of Interdisciplinary Medicine and Biotechnology, Beth Israel Deaconess Medical Center, Boston, Massachusetts, USA.

Shwachman-Diamond syndrome (SDS) is a rare and clinically heterogeneous bone marrow (BM) failure syndrome caused by mutations in the Shwachman-Bodian-Diamond syndrome (*SBDS*) gene. Although SDS was described more than 50 years ago, its molecular pathogenesis is poorly understood due, in part, to the rarity and heterogeneity of the affected hematopoietic progenitors. To address this, we used single-cell RNA sequencing to profile scant hematopoietic stem and progenitor cells from patients with SDS. We generated a single-cell map of early lineage commitment and found that SDS hematopoiesis was left-shifted with selective loss of granulocyte-monocyte progenitors. Transcriptional targets of transforming growth factor beta (TGF-β) were dysregulated in SDS hematopoietic stem cells and multipotent progenitors, but not in lineage-committed progenitors. TGF-β inhibitors (AVID200 and SD208) increased hematopoietic colony formation of SDS patient BM. Finally, TGF-β3 and other TGF-β pathway members were elevated in SDS patient blood plasma. These data establish the TGF-β pathway as a candidate biomarker and therapeutic target in SDS and translate insights from single-cell biology into a potential therapy.

Introduction

Shwachman-Diamond syndrome (SDS) is an inherited bone marrow (BM) failure syndrome associated with biallelic, hypomorphic mutations in the Shwachman-Bodian-Diamond syndrome (*SBDS*) gene. SBDS is a pleiotropic protein that facilitates basic cellular processes such as ribosomal subunit joining and mitotic spindle assembly (1–5). Despite the simple genetic underpinnings of SDS, clinical heterogeneity driven by differences in the primarily affected blood cell lineages complicates diagnosis and treatment. BM failure typically manifests first in the myeloid lineage, but erythroid and megakaryocyte dysfunction may co-occur to varying degrees.

The only curative treatment for BM failure in patients with SDS is hematopoietic stem cell (HSC) transplant. Unfortunately, outcomes are limited by the inability to predict which patients will develop complications, such as progression to clonal disease, that outweigh significant transplant risks. The development of rational therapies that could supplant or delay transplant requires a deeper understanding of the pathways that underlie cell type–specific responses to *SBDS* mutations. These pathways have been difficult to assess due to limitations of animal models and the paucity of human primary cells that can be obtained from BM failure patients. Here, we leverage recent technological advances in single-cell profiling to directly examine the molecular pathogenesis of SDS in primary patient BM. Our findings implicate the transforming growth factor beta (TGF-β) pathway as a potential therapeutic target in SDS and demonstrate the power of single-cell transcriptomics to shed new light on rare and intractable diseases.

Results and Discussion

Despite the basic cellular functions of SBDS, only certain cell types manifest dysfunction in SDS. BM hypocellularity and peripheral cytopenias involving multiple lineages (6, 7) are hallmarks of SDS, suggesting defects in the $CD34^+$ hematopoietic stem and progenitor cell (HSPC) pool. We hypothesized that the dynamic subpopulations that comprise the HSPC pool may exhibit selective responses to *SBDS* mutations that influence clinical presentation. To simultaneously examine the consequences of *SBDS* mutations across HSPC subpopulations, we performed single-cell RNA sequencing (RNA-seq) on $CD34^+$ cells freshly isolated from the BM of healthy donors ($n = 4$, ranging from 25–29 years old) and patients with SDS ($n = 4$, ranging from 11–26 years old). The patients with SDS all exhibited BM hypocellularity or cytopenias at the time of sampling; one patient was being treated with G-CSF for severe neutropenia

Authorship note: CEJ and A. Saadatpour are co–first authors and contributed equally to this work.
Conflict of interest: The authors have declared that no conflict of interest exists.

Submitted: October 9, 2018; **Accepted:** June 11, 2019; **Published:** August 12, 2019.
Reference information: *J Clin Invest*. 2019;129(9):3821–3826.
https://doi.org/10.1172/JCI125375.

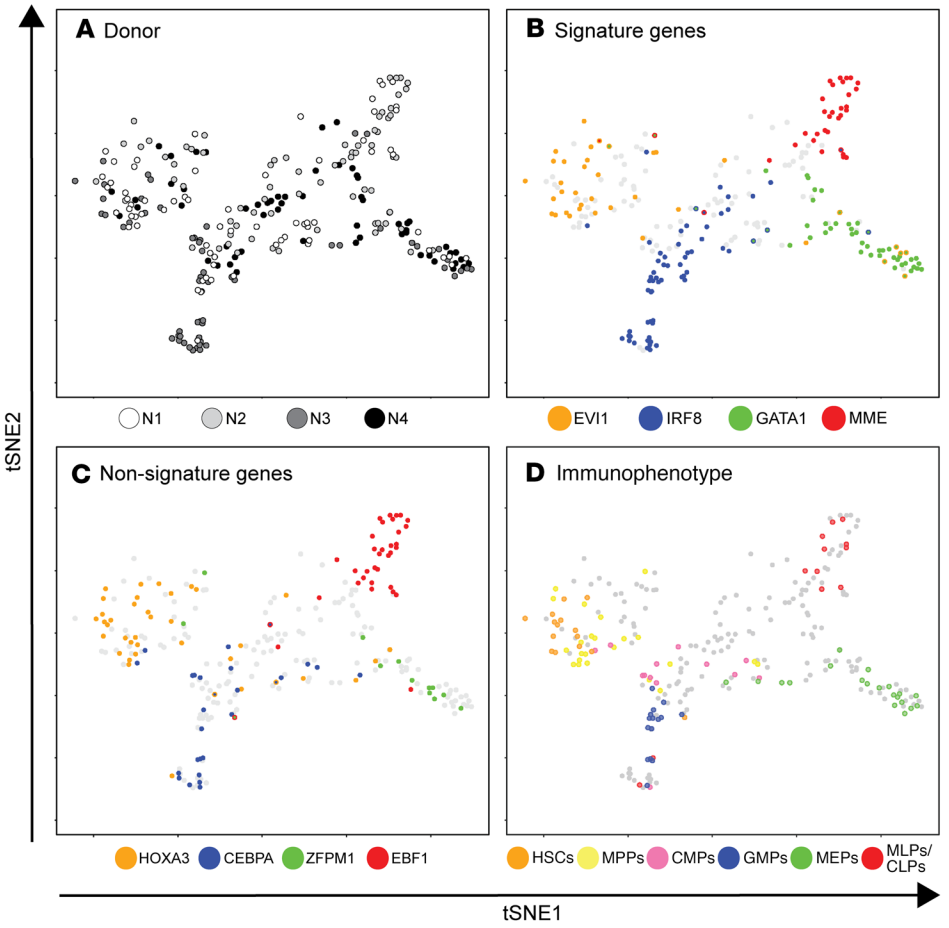

Figure 1. Supervised dimensionality reduction maps lineage commitment of CD34⁺ cells from healthy donors. tSNE plot of hematopoietic lineage commitment was derived from an empirically defined gene expression signature. Shown here are cells from 4 healthy donors (N1: n = 70; N2: n = 58; N3: n = 69; N4: n = 59; N = 256). Cells are colored based on (**A**) donor identity, (**B**) mRNA expression of selected signature genes, (**C**) mRNA expression of lineage-restricted genes reported elsewhere (12), and (**D**) immunophenotypes. For B and C, color indicates TPM >1 for the indicated mRNA enriched in stem (orange), myeloid (blue), erythroid (green), or lymphoid (red) cells. The presence of 2 colors indicates coexpression. Grey indicates TPM <1 for all 4 factors. For D, color indicates membership in a gated immunophenotypic subset as shown in Supplemental Figure 1, A and B. Grey indicates cells that were ungated or sorted without indexing. Numerical axes derived from tSNE are arbitrary, and therefore not shown.

(Supplemental Table 1) and is discussed separately below. We selected CD34⁺ cells from the mononuclear fraction without gating on additional markers, sequenced single cells using the SMART-seq approach for full-length cDNA amplification (Clontech) (8, 9), and classified HSPC a posteriori based on transcriptional signatures of lineage commitment. This approach is well suited to capture cells along the CD34⁺ differentiation spectrum, which is a subject of evolving understanding in human BM (10, 11).

A major challenge for studying a rare patient population is that biological variables and batch effects can obscure disease signatures. To classify single cells with respect to hematopoietic lineage commitment (and not other unrelated variables), we designed a supervised dimensionality reduction analysis. Specifically, we performed bulk RNA-seq on FACS-purified HSPC subpopulations (12) from normal BM to derive an mRNA expression signature that distinguished HSCs, multipotent progenitors (MPPs), common myeloid progenitors (CMPs), multilymphoid progenitors (MLPs), granulocyte-monocyte progenitors (GMPs), and megakaryocyte-erythroid progenitors (MEPs) (Supplemental Figure 1). We then analyzed this signature in single-cell RNA-seq data sets from both normal and SDS BM to predict the identity of each cell. Data were visualized using *t*-distributed stochastic neighbor embedding (tSNE; Figure 1, Supplemental Table 2) (13). For simplicity, SDS cells are masked in Figure 1.

Cells from 4 healthy donors were interspersed in a configuration that suggested population structure related to hematopoietic lineage commitment (Figure 1A). To associate regions of the map with specific lineages, we examined the expression of select mRNAs that are associated with stem, myeloid, erythroid, and lymphoid fate (11). We examined a set of mRNAs that was present in our 79-signature (Figure 1B), and a set that was absent from our signature as independent validation (Figure 1C). Most cells primarily expressed mRNAs associated with one fate, and expression of the different lineage-predictive mRNAs was concentrated in distinct regions of the tSNE map (Figure 1, B and C). To confirm patterns of lineage commitment as determined by mRNA expression, we examined indexed surface marker intensities on a subset of normal cells. Gated HSCs, MPPs, MLPs, CMPs, GMPs, or MEPs accounted for 68% of indexed cells. An additional 9% were CD34⁺CD90⁻CD38⁺CD10⁺CD45RA⁺ common lymphoid progenitors (CLPs). The remaining 23% fell outside of defined gates and possibly represent transitional or unconventional HSPC states. Cells that did fall within defined gates clustered in distinct regions of the map that were consistent with mRNA expression patterns (Figure 1D). Thus, supervised transcriptional mapping distinguished the major branches of hematopoiesis among randomly sampled CD34⁺ cells.

We used this single-cell map of normal hematopoietic lineage commitment as a baseline from which to examine alterations in the cellular architecture of SDS hematopoiesis. Figure 2A shows the same map as in Figure 1, with cells from SDS patients unmasked. SDS and normal cells were intermixed, but their distribution and relative frequencies differed (χ^2 P <

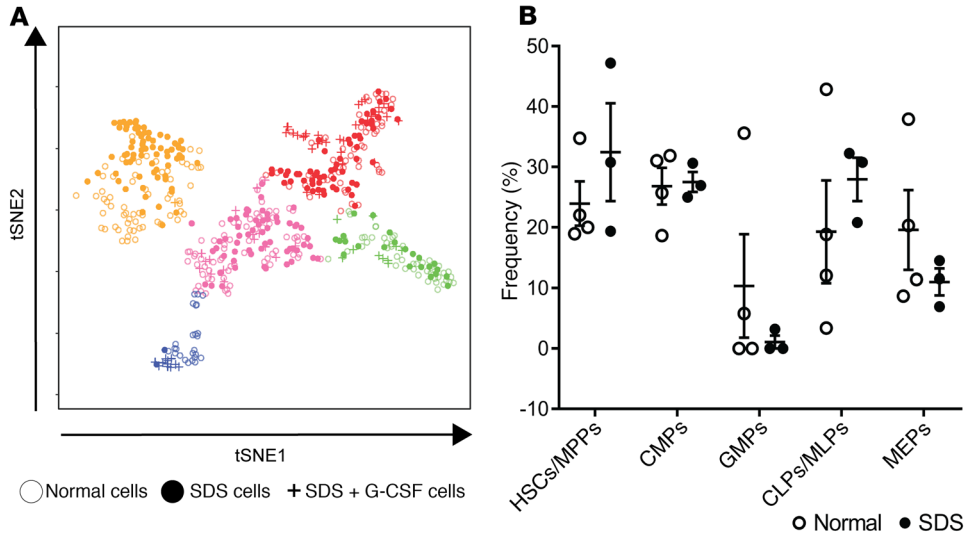

Figure 2. The cellular architecture of early hematopoiesis is altered in SDS. (**A**) tSNE plot of hematopoietic lineage commitment showing cells from healthy donors as in Figure 1, untreated SDS patients (SDS1.1: n = 72; SDS1.2: n = 62; SDS2.1: n = 78; N = 212), and an SDS patient who was being treated with 4.2 μg/kg/day G-CSF (SDS2.2: n = 71). Clusters were determined using the partitioning around medoids version of k-means clustering (k = 5), and labeled based on the enrichment of index-sorted HSCs, MPPs, MLPs, CMPs, GMPs, and MEPs as shown in Figure 1D. The sum of normal cells and SDS cells in each cluster is significantly changed using the χ^2 test. HSCs/MPPs, orange; CMPs, pink; GMPs, blue; CLPs/MLPs, red; MEPs, green. (**B**) Relative frequencies of HSPC subpopulations for healthy donors and untreated SDS patients. Error bars indicate SEM.

0.0001). We quantified these changes using k-means clustering. Five clusters were defined based on maximum silhouette value and named for the most enriched immunophenotypic subpopulation within the cluster (Figure 2A). CMPs, MLPs/CLPs, GMPs, and MEPs each designated a distinct cluster whereas HSCs and MPPs were enriched in the same cluster. Untreated patients with SDS had a stark reduction in GMPs and a modest increase in HSCs/MPPs (Figure 2B). The reduction in GMPs was evident even in the absence of symptomatic neutropenia (Supplemental Figure 2), suggesting that it contributes to the neutropenia predisposition in patients with SDS. G-CSF treatment in one patient rescued loss of GMPs and depleted HSCs/MPPs from the BM (Figure 2B), consistent with the drug's known mechanism (14). We therefore excluded cells from this treated patient from comparative gene expression analyses.

We next compared gene expression between normal and SDS cells within each cluster except for GMPs, which was excluded due to the low number of GMPs in untreated patients with SDS. Overall, 1680 genes were differentially expressed in at least one cluster (FDR < 0.05, $\log_2$ [fold change] > 1; Supplemental Table 3). Strikingly, 81.5% of all differentially expressed genes were unique to either HSCs/MPPs or CMPs (Figure 3A). An additional 9.8% were commonly affected in HSCs/MPPs and CMPs, but not in MLPs/CLPs or MEPs. Overall, these data demonstrate that despite the general biochemical functions of the SBDS protein, *SBDS* mutations differentially affect the frequency (as for GMPs) or gene expression characteristics (as for HSCs/MPPs or CMPs) of HSPC subpopulations. In contrast, the MLP/CLP and MEP populations are relatively unaffected.

The inflammatory response was enriched among differentially expressed genes in both the HSC/MPP and CMP clusters (maximum P value 4.98×10^{-5} and 1.18×10^{-3}, respectively). However, the genes contributing to the enrichment differed between the clusters (Figure 3B). TGF-β was the top regulator predicted for the HSC/MPP inflammatory response (P = 4.03×10^{-15}, Z score = 0.891). It was also a significant upstream regulator among all differentially expressed genes in HSCs/MPPs (P = 1.27×10^{-2}, Z score = 0.417). Dysregulation of these TGF-β targets was most significant in HSCs/MPPs, with lesser or no effect in other HSPC populations (Figure 3C). TGF-β induces context-dependent effects on cell growth, survival, inflammation, and extracellular matrix. TGF-β1 and TGF-β3 have potent growth inhibitory effects on HSCs (15–17). Thus, we hypothesized that activation of TGF-β in SDS HSCs/MPPs may contribute to BM failure in patients with SDS.

To confirm activation of TGF-β signaling in BM from patients with SDS, we assessed TGF-β–dependent phosphorylation and nuclear translocation of the transcriptional coactivator protein mothers against decapentaplegic homolog 2 (p-SMAD2). A subset of $CD34^+$ cells from BM from SDS patients had elevated levels of nuclear p-SMAD2 that were outside the normal range (Figure 4, A and B). Treating SDS cells with AVID200, a decoy receptor trap designed to specifically neutralize TGF-β1 and TGF-β3, reduced the p-SMAD2 signal. The same trend was observed to varying degrees in 2 additional sample pairs (Figure 4C). These data are consistent with our single-cell RNA-seq analysis demonstrating selective activation of the TGF-β pathway in the HSC/MPP subset of SDS $CD34^+$ cells.

BM cells from SDS patients exhibit impaired hematopoietic colony formation in vitro (18) (Supplemental Figure 3A). To determine whether attenuation of TGF-β signaling improves SDS hematopoiesis, we cultured primary BM mononuclear cells from patients with SDS and healthy donors (Supplemental Table 1) in methylcellulose supplemented with AVID200 and SD208, which inhibits TGF-βR1 kinase activity (19). Both compounds improved hematopoietic colony formation in SDS patient samples, but not in healthy donor controls (Figure 4D, Supplemental Figure 3B, Supplemental Table 4). Taken together, our data support a model in which activation of TGF-βR1 kinase activity by TGF-β1 and/or TGF-β3 led to increased concentration of p-SMAD2 in the nucleus and transcription of inflammatory response genes in SDS HSCs/MPPs (Figure 4E).

To determine whether patients with SDS express elevated levels of TGF-β ligands, we screened blood plasma proteins from 6 patients with SDS and 6 healthy controls (Supplemental Table 1) using SOMAscan; a highly sensitive, aptamer-based proteomic platform (20). TGF-β3 was significantly (P = 0.009, Supplemen-

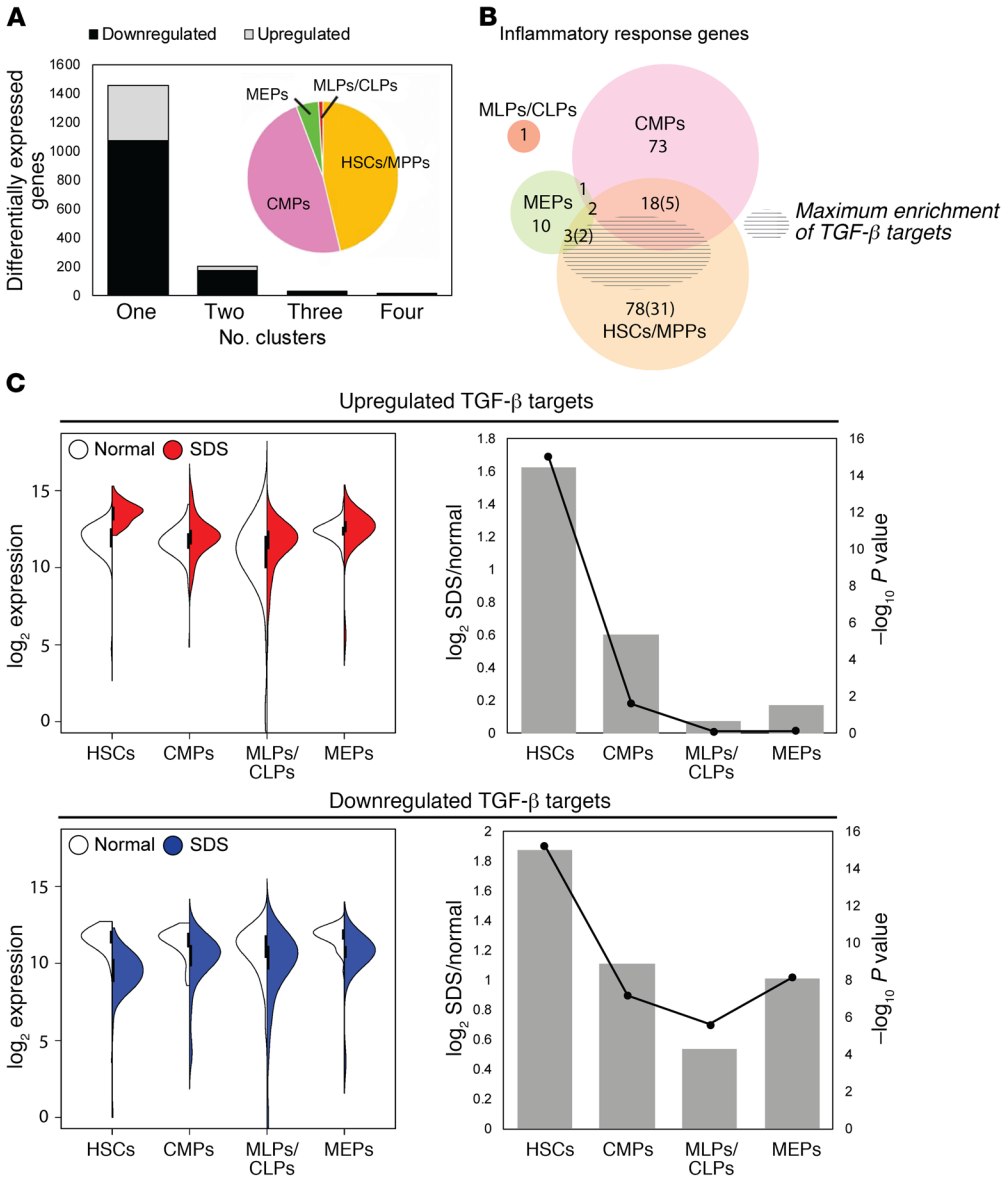

Figure 3. TGF-β signaling is selectively activated in SDS stem and multipotent progenitors. (**A**) Differentially expressed genes were identified among all SDS versus normal cells and within each cluster: HSC/MPP, CMP, MLP/CLP, or MEP. To aid biological interpretation, this gene set was filtered to focus on genes with FDR-adjusted *P* value less than .05 and $\log_2$ (fold change) greater than 1 in at least one cluster. Plotted are the number of genes that were either up- or downregulated in 1, 2, 3, or 4 clusters. The GMP cluster was excluded due to the paucity of SDS GMPs. Inset pie chart shows the proportion of differentially expressed genes in each cluster. (**B**) Venn diagram of differentially expressed genes in each cluster that were annotated to the inflammatory response function in Ingenuity Pathway Analysis. The shaded region shows the area of maximal enrichment of TGF-β targets ($P = 4.03 \times 10^{-15}$). (**C**) Left: split violin for the summed expression of 25 upregulated TGF-β targets and 52 downregulated TGF-β targets in SDS HSCs/MPPs. Right: $\log_2$ fold changes (primary axis, bars) and *P* values (secondary axis, lines) for the gene sets plotted in B. Significance was determined by 2-way ANOVA, with Holm-Sidak's multiple comparisons test.

tal Table 5) upregulated in SDS patient plasma, along with several other factors that were annotated to a network of TGF-β–associated factors (Supplemental Figure 4). These and other dysregulated plasma proteins that were common across clinically heterogeneous patients could serve as diagnostic biomarkers for SDS (Supplemental Table 5). Additional studies are required to determine the levels of TGF-β3 in the BM compartment and identify the cell types that produce it.

Although SDS was reported more than 50 years ago and progress has been made using animal and cellular models (3, 21–23), the molecular mechanisms leading to BM failure remain unclear. Here we leveraged advanced single-cell technologies to perform the first direct analysis of primary human SDS hematopoietic progenitors. Whereas most single-cell transcriptomic studies have focused on dissecting and characterizing cell types (24–27), this study demonstrates the power of single-cell transcriptomics to uncover a key disease mechanism in rare cells. Our data add to an emerging body of evidence linking inflammation to BM dysfunction, including Fanconi anemia (FA) where the pathogenic mechanism of TGF-β is thought to be suppression of homologous

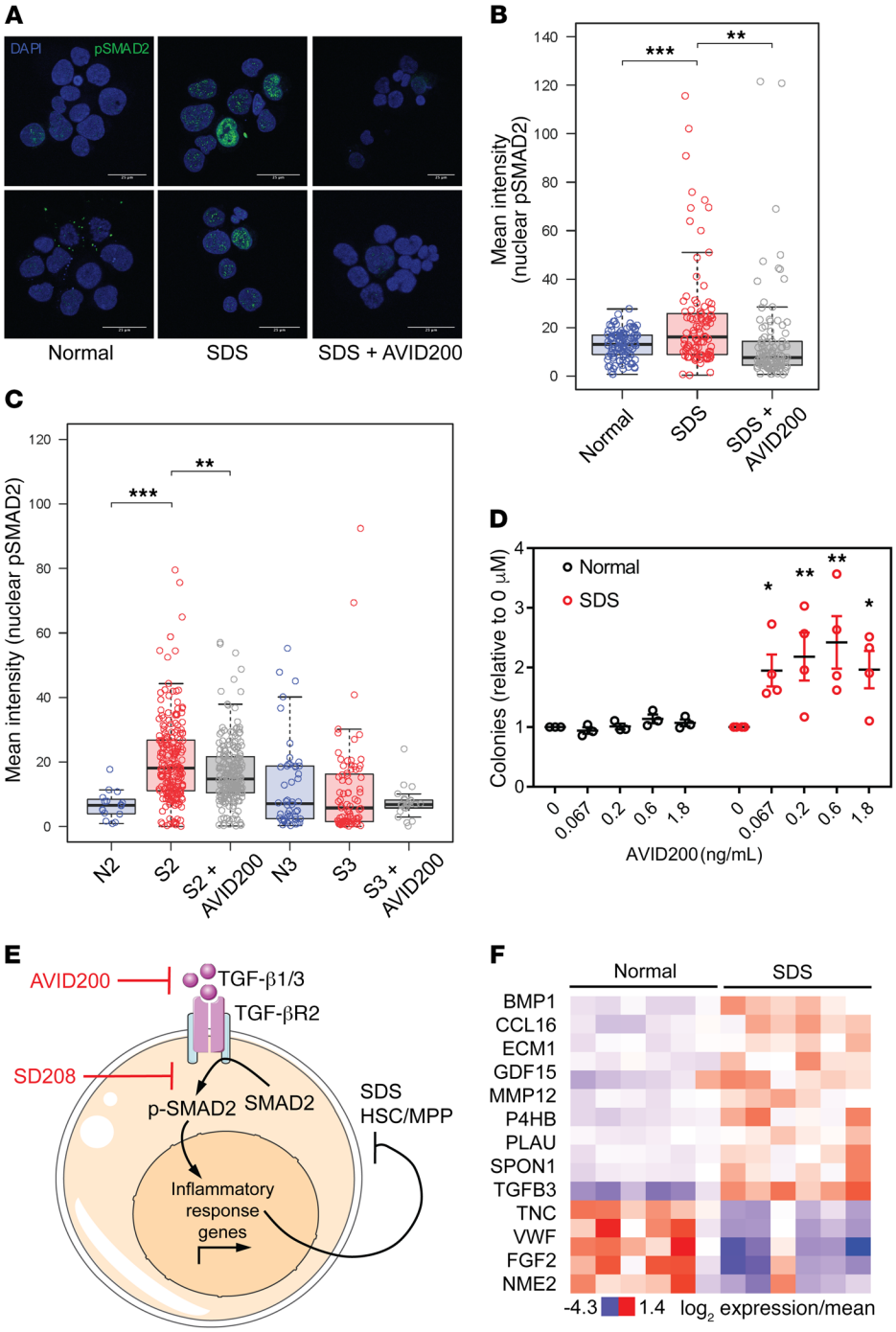

Figure 4. TGF-β pathway activation through TGF-βR1 suppresses hematopoiesis in SDS BM progenitors. (**A**) Representative images showing DAPI and phospho-SMAD2 staining of primary BM CD34⁺ cells from adult healthy donor BM and pediatric SDS BM, either untreated or treated with AVID200. Scale bar: 25 μm. (**B**) Mean intensity of phospho-SMAD2 staining in individual CD34⁺ nuclei from samples depicted in A. Significance was determined by 2-way ANOVA, with Holm-Sidak's multiple comparisons test. Error bars indicate minimum and maximum values, excluding outliers that exceed median + 1.5*IQR. $^{**}P < 0.01$; $^{***}P < 0.001$. (**C**) Mean intensity of phospho-SMAD2 staining in individual CD34⁺ nuclei in 2 additional pairs of SDS and healthy donor BM samples. Error bars indicate minimum and maximum values, excluding outliers that exceed median + 1.5*IQR. $^{**}P < 0.01$; $^{****}P < 0.0001$. (**D**) Number of colonies formed by adult healthy donor and pediatric SDS patient BM-derived mononuclear cells with increasing concentrations of AVID200, normalized to the 0 μM treatment. Significance was determined relative to the 0 μM treatment by 2-way ANOVA, with Holm-Sidak's multiple comparisons test. Error bars indicate SEM. $^{*}P < 0.05$; $^{**}P < 0.01$. (**E**) Model for the role of TGF-β signaling in SDS BM failure. TGF-β1 and/or TGF-β3 ligands (targets of AVID200 inhibitor) activate signaling through the TGF-βR1 receptor (target of SD208 inhibitor) on SDS HSCs/MPPs. Our data suggest that TGF-β ligands are primarily derived from a CD34⁻ cell type in BM because TGF-β ligand mRNAs were not detected in CD34⁺ HSPCs. Increased TGF-βR1 signaling leads to increased concentrations of nuclear phospho-SMAD2 and transcription of inflammatory response genes, which impairs HSC/MPP function. This model predicts that therapeutic inhibition of TGF-β signaling in HSCs/MPPs will improve hematopoietic function in patients with SDS. (**F**) Expression of extracellular proteins annotated to a TGF-β network that was enriched among dysregulated proteins in SDS patient plasma.

recombination repair (28, 29). We demonstrate a broader role for TGF-β in a mechanistically distinct BM failure syndrome. TGF-β inhibitors are already in clinical trials to treat myelodysplastic syndrome, cancer, and pulmonary fibrosis, among others (30). Our work suggests that TGF-β1/3 inhibition by an agent such as AVID200 could be an effective therapy across clinically heterogeneous patients with SDS and different marrow failure disorders.

Methods

Detailed methods are provided in the Supplemental Material.

Study approval. Subjects provided written, informed consent for protocols approved by the institutional review board of Boston Children's Hospital and Dana-Farber Cancer Institute, in accordance with the Declaration of Helsinki's Ethical Principles of Medical Research Involving Human Subjects. All subjects provided informed consent prior to their participation in the study.

Data processing and availability. Paired-end reads were mapped to the hg38 human transcriptome (Gencode v24) using STAR v2.4.2a. Aligned reads were deposited in and are available through the database of Genotypes and Phenotypes (dbGaP) (phs001845.v1.p1). Gene expression levels were quantified as transcript-per-million (TPM) in RSEM. Cells with at least 1000 expressed genes

(defined by TPM >1) and genes expressed in at least 50 single cells were kept. This resulted in 11,094 genes in 583 single cells. The same set of 11,094 genes was analyzed to derive lineage signature genes from 100 cell libraries made from FACS-purified $CD34^+$ subsets.

Author contributions

CEJ, CN, A. Shimamura, and CDN designed experiments. IH, CAS, A. Shimamura, MRG, JW, and KCM collected patient samples and clinical information. CEJ, MRG, OVB, and DDT performed experiments. A. Saadatpour, LJ, and SY performed computational analyses. CEJ, A. Saadatpour, MRG, OVB, CDN, A. Shimamura, GCY, and TAL analyzed data. CEJ and CDN wrote the manuscript. All authors provided critical reviews of the manuscript.

Acknowledgments

This work was supported by a Department of Defense Idea Award W81XWH-14-1-0124 and NIH grant 1R01 DK102165 to CDN; NIH grant R24 DK099808 to A. Shimamura; and a Claudia Adams Barr Award from the Dana-Farber Cancer Institute to GCY. CEJ was supported by NIH training grant T32 CA070083, a postdoctoral fellowship F32 HL124941, and a Claudia Adams Barr Award from the Dana-Farber Cancer Institute. We thank Formation Biologics for supplying AVID200. We thank Donna Neuberg for critical scientific advice. We thank the Dana-Farber Cancer Institute Flow Cytometry Core, especially John Daley, Michael Buonopane, and Alexander Heubeck, for providing technical expertise and equipment; Broad Technology Labs, especially Jim Bochicchio and Caroline Cusick, for providing project management support; the Beth Israel Deaconess Medical Center Genomics, Proteomics, Bioinformatics and Systems Biology Center, especially Simon T. Dillon, Xuesong Gu, and Hasan Out, for providing technical and analytical support; and the Broad Genomics Platform.

Address correspondence to: Carl D. Novina, Dana-Farber Cancer Institute, Dana 1420B, 450 Brookline Avenue, Boston, Massachusetts 02215, USA. Phone: 617.582.7961; Email: carl_novina @dfci.harvard.edu.

1. Menne TF, et al. The Shwachman-Bodian-Diamond syndrome protein mediates translational activation of ribosomes in yeast. *Nat Genet*. 2007;39(4):486–495.
2. Ganapathi KA, et al. The human Shwachman-Diamond syndrome protein, SBDS, associates with ribosomal RNA. *Blood*. 2007;110(5):1458–1465.
3. Finch AJ, et al. Uncoupling of GTP hydrolysis from eIF6 release on the ribosome causes Shwachman-Diamond syndrome. *Genes Dev*. 2011;25(9):917–929.
4. Burwick N, Coats SA, Nakamura T, Shimamura A. Impaired ribosomal subunit association in Shwachman-Diamond syndrome. *Blood*. 2012;120(26):5143–5152.
5. Austin KM, et al. Mitotic spindle destabilization and genomic instability in Shwachman-Diamond syndrome. *J Clin Invest*. 2008;118(4):1511–1518.
6. Huang JN, Shimamura A. Clinical spectrum and molecular pathophysiology of Shwachman-Diamond syndrome. *Curr Opin Hematol*. 2011;18(1):30–35.
7. Myers KC, et al. Variable clinical presentation of Shwachman-Diamond syndrome: update from the North American Shwachman-Diamond Syndrome Registry. *J Pediatr*. 2014;164(4):866–870.
8. Ramsköld D, et al. Full-length mRNA-Seq from single-cell levels of RNA and individual circulating tumor cells. *Nat Biotechnol*. 2012;30(8):777–782.
9. Picelli S, Björklund ÅK, Faridani OR, Sagasser S, Winberg G, Sandberg R. Smart-seq2 for sensitive full-length transcriptome profiling in single cells. *Nat Methods*. 2013;10(11):1096–1098.
10. Notta F, Doulatov S, Laurenti E, Poeppl A, Jurisica I, Dick JE. Isolation of single human hematopoietic stem cells capable of long-term multilineage engraftment. *Science*. 2011;333(6039):218–221.
11. Velten L, et al. Human haematopoietic stem cell lineage commitment is a continuous process. *Nat Cell Biol*. 2017;19(4):271–281.
12. Laurenti E, et al. The transcriptional architecture of early human hematopoiesis identifies multilevel control of lymphoid commitment. *Nat Immunol*. 2013;14(7):756–763.
13. van der Maaten L, Hinton G. Visualizing high-dimensional data using t-SNE. *J Mach Learn Res*. 2008;9(Nov):2579–2605.
14. Thomas J, Liu F, Link DC. Mechanisms of mobilization of hematopoietic progenitors with granulocyte colony-stimulating factor. *Curr Opin Hematol*. 2002;9(3):183–189.
15. Hatzfeld J, et al. Release of early human hematopoietic progenitors from quiescence by antisense transforming growth factor beta 1 or Rb oligonucleotides. *J Exp Med*. 1991;174(4):925–929.
16. Scandura JM, Boccuni P, Massagué J, Nimer SD. Transforming growth factor beta-induced cell cycle arrest of human hematopoietic cells requires p57KIP2 up-regulation. *Proc Natl Acad Sci U S A*. 2004;101(42):15231–15236.
17. Challen GA, Boles NC, Chambers SM, Goodell MA. Distinct hematopoietic stem cell subtypes are differentially regulated by TGF-beta1. *Cell Stem Cell*. 2010;6(3):265–278.
18. Dror Y, Freedman MH. Shwachman-Diamond syndrome: An inherited preleukemic bone marrow failure disorder with aberrant hematopoietic progenitors and faulty marrow microenvironment. *Blood*. 1999;94(9):3048–3054.
19. Uhl M, et al. SD-208, a novel transforming growth factor beta receptor I kinase inhibitor, inhibits growth and invasiveness and enhances immunogenicity of murine and human glioma cells in vitro and in vivo. *Cancer Res*. 2004;64(21):7954–7961.
20. Gold L, Walker JJ, Wilcox SK, Williams S. Advances in human proteomics at high scale with the SOMAscan proteomics platform. *N Biotechnol*. 2012;29(5):543–549.
21. Tourlakis ME, et al. Deficiency of Sbds in the mouse pancreas leads to features of Shwachman-Diamond syndrome, with loss of zymogen granules. *Gastroenterology*. 2012;143(2):481–492.
22. Zambetti NA, et al. Deficiency of the ribosome biogenesis gene Sbds in hematopoietic stem and progenitor cells causes neutropenia in mice by attenuating lineage progression in myelocytes. *Haematologica*. 2015;100(10):1285–1293.
23. Tulpule A, et al. Pluripotent stem cell models of Shwachman-Diamond syndrome reveal a common mechanism for pancreatic and hematopoietic dysfunction. *Cell Stem Cell*. 2013;12(6):727–736.
24. Villani AC, et al. Single-cell RNA-seq reveals new types of human blood dendritic cells, monocytes, and progenitors. *Science*. 2017;356(6335):eaah4573.
25. Tirosh I, et al. Dissecting the multicellular ecosystem of metastatic melanoma by single-cell RNA-seq. *Science*. 2016;352(6282):189–196.
26. Kumar RM, et al. Deconstructing transcriptional heterogeneity in pluripotent stem cells. *Nature*. 2014;516(7529):56–61.
27. Darmanis S, et al. A survey of human brain transcriptome diversity at the single cell level. *Proc Natl Acad Sci U S A*. 2015;112(23):7285–7290.
28. Zhang H, et al. TGF-β inhibition rescues hematopoietic stem cell defects and bone marrow failure in Fanconi anemia. *Cell Stem Cell*. 2016;18(5):668–681.
29. Zhou L, et al. Reduced SMAD7 leads to overactivation of TGF-beta signaling in MDS that can be reversed by a specific inhibitor of TGF-beta receptor I kinase. *Cancer Res*. 2011;71(3):955–963.
30. Herbertz S, et al. Clinical development of galunisertib (LY2157299 monohydrate), a small molecule inhibitor of transforming growth factor-beta signaling pathway. *Drug Des Devel Ther*. 2015;9:4479–4499.